International Journal of Marine Engineering Innovation and Research, Vol. 11(1), Mar. 2026. 147-156
(pISSN: 2541-5972, eISSN: 2548-1479)

Improvement of Impinging Jet Casing Design On Savonius Turbine Performance

Amron Rosyada[1*], Achmad Baidowi [2], Sunarsih [3]

(Received: 27 January 2026 / Revised: 12 February 2026 / Accepted: 13 February 2026 / Available Online: 7 March 2026)

***Abstract*—** Savonius turbine is one of the various devices used to convert fluid flow energy into electricity. Due to its low efficiency, many studies have been performed to increase its performance including the utilization of ducting/casing system. In this paper, a further investigation into the effect of the lower plate duct stream direction from previous casing design is conducted. There are 4 casing designs; base casing design (BCD) from previous work and 3 proposed designs. The proposed designs have impinging jet stream direction perpendicularly with the concave side of returning blade azimuth position of 60° (D-I), 75° (D-II), and 90° (D-III) respectively. The study employed two-dimensional CFD (Computational Fluid Dynamic) transient method using Ansys Fluent with Kω-SST (Shear-Stress Transport) as the turbulence model. The results show that all duct designs are able to rise up the coefficient of power (Cp) of conventional turbine design. Furthermore, D-III and D-II have better performance than BCD at all tip speed ratios (TSRs). D-III surpasses BCD's peak performance at TSR =1 by 8%. By applying D-III casing design, the best conventional turbine Cp (23%) can be improved up to 43% at the same working condition (TSR=0.8). Additionally, the shorter flow passage could increase the impinging jet stream velocity.

Keywords—Azimuth Position, impinging jet, savonius turbine.

[*]*Corresponding Author: rosyadaamron@gmail.com*

I. INTRODUCTION

Savonius turbine is one of the various devices used to convert fluid flow energy into electricity. The principal working principle of a Savonius turbine is to capture the drag force generated by the fluid stream using its blades and then convert it into rotational motion (torque). Therefore, maximum torque generation is theoretically achieved when the effective drag force is normal to the blade surface. This cross-flow vertical axis turbine type is highly reliable to be applicated in low stream water flow such as canal and river. Moreover, savonius turbine has several advantages; simple design, low manufacture cost, high starting torque, and not requiring sealed water transmission. In another hand, the efficiency of this turbine is low [1] due to the presence of negative torque on the returning blade. Several enhancements have been studied by many researchers. One of which is the implementation of external structure designs such as deflector plate and ducting.

Alizadeh et al. [2] added a simple deflector plate in front of the returning blade to deflect the water stream and improve the turbine's generated power. A numerical study using CFD was conducted to investigate the optimum length of the deflector plate. It was found that using the optimum deflector length could increase the maximum generated power by approximately 18%. Mosbahi et al. [3] experimentally studied a helical Savonius turbine in an irrigation channel. Subsequently, a new deflector system consisting of an airfoil-like shape and a plate was added to enhance the turbine's performance. This second step was carried out using 3D CFD simulations. The results showed that the use of the deflector increased the turbine's maximum power coefficient from 0.125 to 0.14. Setiawan et al. [4] numerically analyzed the impact of adding a circular cylinder near the advancing blade on the performance of a Savonius water turbine using CFD simulations. The cylinder diameter was varied. It was found that increasing the cylinder diameter enhanced the performance of the conventionally designed turbine. Furthermore, the maximum power coefficient improved by approximately 18.04%.

The use of a deflector plate is indeed able to improve the performance of a Savonius turbine; however, the use of a ducting system can generate greater performance enhancement [1]. One of the ducting system designs is the impinging jet duct, which was proposed by El-Askary et al [5]. The design was aimed to create fluid jet toward the concave side of both advancing blade and returning blade. His optimum design could generate up to 52% efficiency, a better performance than conventional savonius turbine with only 10%. Thakur et al [6] utilized the impinging jet design on water flow use. The result reveals a rise on power extracted by turbine by approximately 82% better than based design (17 W) at 1.5 m/s water velocity. Improvement attempts to this impinging jet design have been performed by Antar and Elkhoury [7]. They varied the radius factors of the duct passages both on upper plat and lower plate. The optimized design is capable of producing 48% better performance than the baseline casing design. However, the direction of the water flow from the lower plate toward the concave side of the returning blade has not yet been explicitly studied. In this paper, further observation of impinging jet geometry is performed which is the effect of impinging jet direction to the concave side of returning as the main idea. The

Amron Rosyada is with Departement of Marine Engineering, Institut Technologi Sepuluh Nopember, Surabaya, 60111, Indonesia. E-mail: rosyadaamron@gmail.com

Achmad Baidowi is with Departement of Marine Engineering, Institut Technologi Sepuluh Nopember, Surabaya, 60111, Indonesia. E-mail: achmad.baidowi@its.ac.id

Sunarsih is with Departement of Marine Engineering, Institut Technologi Sepuluh Nopember, Surabaya, 60111, Indonesia. E-mail: sunarsih@its.ac.id

proposed designs, which consider perpendicular flow onto the concave surface of the returning blade, are presented in the following section.

II. GEOMETRY AND CASING DESIGNS

Turbine model studied in this research is based from Gallo et al [8]. It is a 2-bladed turbine having 200 mm diameter (D), zero overlap ratio (OR), and 1 mm blade plate thickness. For the impinging jet casing, there are 4 model of casings. The first one is the base casing design (BCD) proposed by El-Askary et al [5]. The rest models are the proposed models that are being analyzed in present study. The first proposed design has lower plat that guides fluid towards the concave side of returning blade perpendicularly when the blade position is at 60° (D-I) while others are perpendicularly with 75° (D-II) and 90° (D-III) blade azimuthal position. The modification parts are colored by red. The casing geometry sizes are measured in radius (R) function (see Figure 1). The idea of the proposed models in this study is to shorten the impinging jet passage in order to preserved the kinetic energy of the stream and to investigate the effect of the incoming jet stream directions to the turbine performance. Hence, the entrance and impinging jet passage widths are maintained the same, 5.7R and 0.5R respectively. The casing plate thickness is assumed as 3 mm [6].

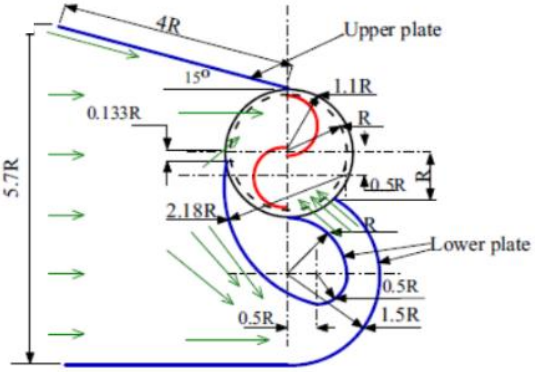

(a)

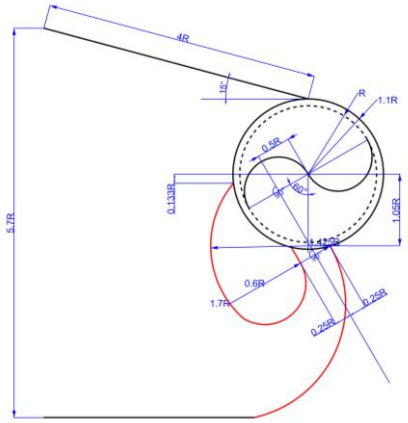

(b)

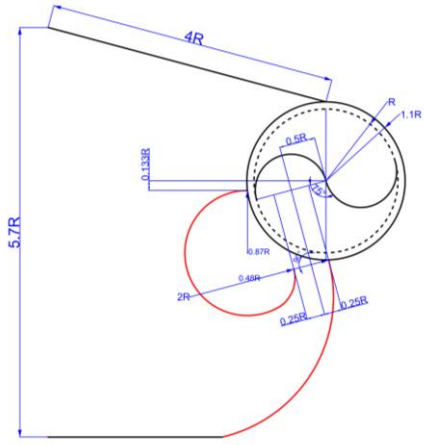

(c)

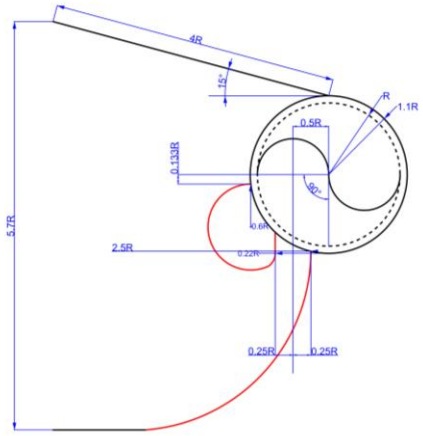

(d)

Figure 1. Impinging Jet Casing Designs, (a) BCD (El-Askary [5]), (b) D-I, (c) D-II, and (d) D-III

III. METHOD

This present study conducts CFD analysis using Ansys Fluent software. The simulation is based on transient mesh motion method which has abilities to catch turbulence effect and offers reliable result [9]. Additionally, this method has been widely employed on vertical axis turbine analysis [10] [11] [12] [13].

A. Domain and Meshing

The domain consists of three regions; stationary zone, wake zone, and rotating zone. Each zone is connected by "shared topology" in Ansys Spaceclaim. This method allows the connection of mesh nodes between two adjacent domains. The fluid domain size is 5D x 10D with the turbine located in the center which can be seen in Figure 2a. The left side of the domain is assigned as inlet while the right side is the outlet. The rest sides are assigned as symmetry to eliminate blockage ratio effect. This domain configuration is used for validating turbine model and Ansys setup. Therefore, it is a necessary to mimic the domain size of the source paper since it can affect the simulation result [14]. However, a bigger domain size is needed to observe the turbine performance clearer and to accommodate the casings geometry.

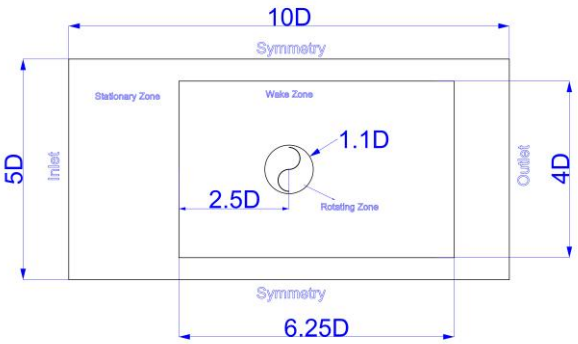

(a)

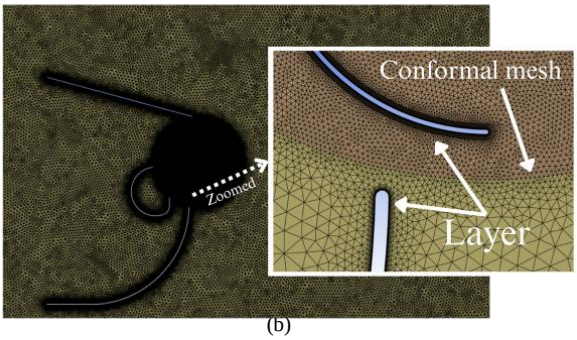

(b)

Figure 2. (a) First Domain and (b) Triangular Mesh

Thus, in the second domain, the stationary domain is extended. As the result, the domain size becomes 10D x 15D [5] [6]. Quad mesh is applied to the stationary zone. This is mainly because quad mesh has advantage of good skewness and less cell numbers. For the rest zones, triangular mesh has been applied because of its ability to adapt with complex geometry such as blade and casing shape. Furthermore, the inflation technique is assigned to all walls with 10 layers and 5 x 10^{-5} m first layer height in order to keep y+ < 1. This result is presented in Figure 2b.

B. Simulation Setup

The transient sliding mesh simulation has been carried out in this study. In sliding mesh technique, the rotating domain will rotate in particular angular speeds (ω). Hence, the slitting technique has been performed into the rotating region. K-ω SST has been chosen for turbulence method since it could give accurate result and has better capabilities of flow separation prediction [15] [16]. The inlet is treated as velocity inlet while the outlet boundary is assigned as pressure outlet. The flow velocity is equal to Re = 48600 [8] for validating the model. However, for further investigation, the water velocity is set as 0.5 m/s with *TSR* ranged from 0.4 up to 1.6. All walls are treated as no-slip walls and only turbine blade is treated as a moving wall with rotational speed adjusted to the rotating zone. Since this is a 2D analysis, it is important to set the reference value to get the moment of coefficient (*Cm*). The depth (*H*) is set as 1 m. as the result, the area (*A=DH)* is 0.2 m^2. The length is turbine radius which is 0.1 m. The reference value is computed from inlet with the rotating zone as the reference zone.

SIMPLE (Semi-Implicit Pressure Linked Equations) algorithm is chosen to estimate the pressure–velocity coupling. A second-order upwind scheme is adopted for the discretization of momentum, turbulent kinetic energy, and specific dissipation rate to run governing equations' spatial discretization. This scheme could give more accuracy than first-order upwind scheme. The criterion of convergence is based on the residual value of 10^{-3} for all variables [17] [18] [19] [10] [7]. In order to minimize the transient effect, the *Cm* is calculated based on the average value after three turbine rotation until ten rotations [7]. The time step size (TSS) is determined by how much times needed for 1° turbine rotation. Eq.1 shows the formula to calculate TSS.

$$TSS = 2\pi\theta/360\omega \quad (1)$$

Where, θ is 1° and ω is angular speed of turbine

C. Grid Independent Test

Mesh or grid independent test is important to be conducted in order to minimize the effect of mesh number to the results. Since there are two domain schemes, GIT has been done for each domain. The first domain shows that after 1.76 x 10^5 cells the *Cp* relatively the same as depicted in Figure 3a. while on the extended domain, the numbers of cells chosen as minimum threshold is 1.96 x 10^5 (see Fig.3b).

D. Data Reduction

The numerical investigation is aim to get the efficiency of the turbine designs. This efficiency is expressed into coefficient of power (*Cp*) which can be calculated by using eq.2 [20].

$$Cp = Cm \cdot TSR \quad (2)$$

Cm is the representation of how much torque (T) that turbine is able to generate relatively to the kinetic energy of the flow stream while *TSR* is ratio between rational speed (ω) at the tip of the blade and the incoming fluid velocity (V).

$$Cm = T/(0.5\rho ARV^2) \quad (3)$$

$$TSR = \omega R/V \quad (4)$$

Torque produced by turbine (T) can be computed by using eq.5 [21].

$$T = \sum_f (F_{f\_pressure} + F_{f\_shear}) \cdot l = \sum_f ((p_f - p_{ref})A_f + (-\tau \cdot A_f))_{(concave)} \cdot l - ((p_f - p_{ref}) \cdot A_f + (\tau \cdot A_f))_{(convex)} \quad (5)$$

Where $F_{f\_pressure}$ and F_{f_shear} are pressure and shear force respectively affecting area A_f while *l* is an arm of torque vector. Reynold number (Re), in addition, takes a crucial role in turbine performance. It is a dimensionless quantity that represents flow behavior. Reynold number can be expressed by eq.6

$$Re = \rho VD/\mu \quad (6)$$

Where ρ is fluid density and μ is dynamic viscosity.

IV. Results and Discussion

A. Validation

Before starting the main analysis, it is crucial to validate the model and the numerical setup based on the point of interest which is *Cp* in this study. The reason behind this is to get data which are comparable and clearly able to see the impact of the modification applications. The maximum deviation allowed is 5%. Fig 4 presents the comparison of *Cp* vs *TSR* between present study and resource paper by Gallo et al [8]. Considering that the resource paper used air as the working fluid, this validation process conducts two types of fluids, air and water, with the same Reynold number (Re = 48600) which are equal to 4 m/s air flow velocity and 0.244 m/s water flow velocity. Both arrangements yield under 4% maximum deviations of *Cp* compared to the source study. This is in accordance with Salleh et al work [22] that with similar Reynold number, type of working fluid provides no significant effect on turbine power performance. As the result, the geometry and the computational setup configurations in this present study can reasonably be deemed its validity.

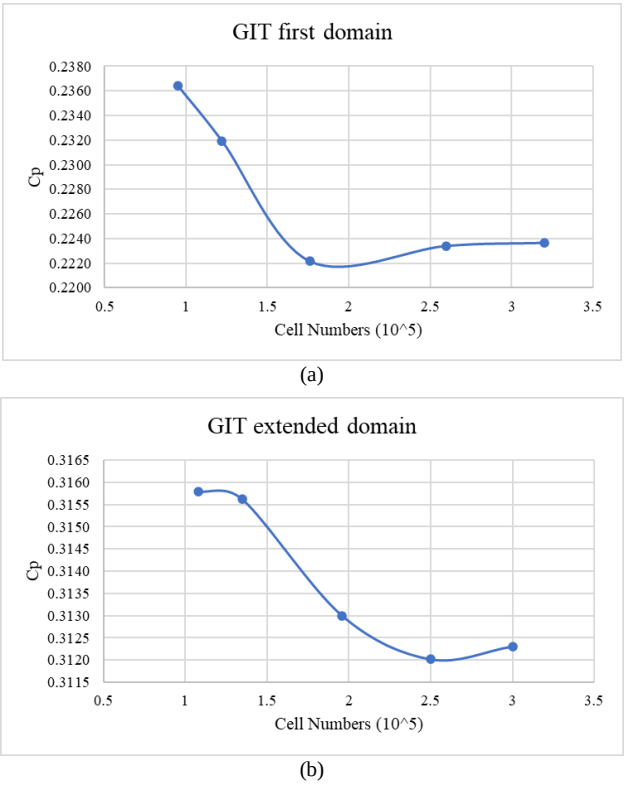

Figure 3. Grit Independent Test, (a) first domain and (b) extended domain

B. Coefficient of Moment

Fig 4 shows that all turbine with casing designs have higher peak of *Cm* than the conventional or caseless design. Furthermore, casing design 4 has the widest positive *Cm* zone under the curve among other designs. This means that the turbine could convert fluid flows energy into mechanical motion better than other turbine designs. Another plus point is that it has the smallest dip to negative *Cm* after 180 azimuth position in short period. Negative *Cm* indicates negative torque and could appears as the pressure difference on returning blade is higher than on the advancing blade. On caseless turbine, for example, shows wide area of negative *Cm* at some azimuth position ranges. This because the returning blade is exposed to flow stream and creates drag force which is bigger than drag force on its advancing blade. Since the positive *Cm* has wider area under the curve than the negative *Cm*, the turbine still could generate positive net torque. Other interesting behaviors happen at azimuth turbine of 45°-120° and 240° - 310° where *Cm* of caseless design is higher than the turbine with casings. The reason behind this will be elucidated in following sections.

Figure 5 depicts the average *Cm* obtained from each *TSR*. In conventional savonius turbine cases, the *Cm* is declining as the *TSR* is inclining. However, applicating the impinging jet casing gives hill-like curve. After *TSR* = 4 to *TSR* = 1, the *Cm* values are relatively constant on turbine with casing designs except D-I which its peak *Cm* happens at *TSR* = 0.8 then drops quickly. Both D-II and D-III drop *Cm* at high *TSR*. Furthermore, D-III has overal better *Cm* than others.

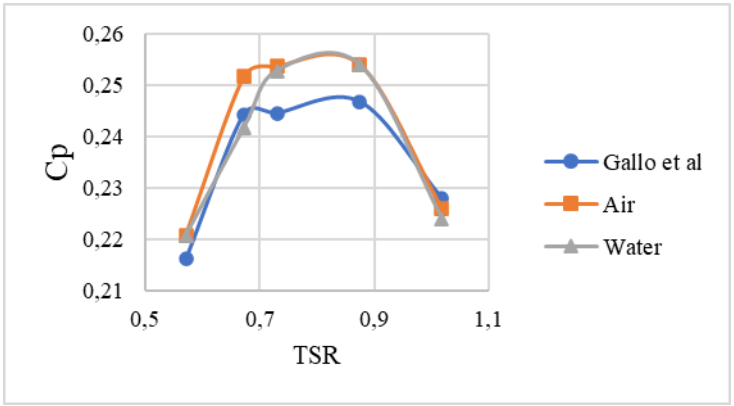

Figure 4. Comparison of *Cp* vs *TSR* Between Previous and Present Work

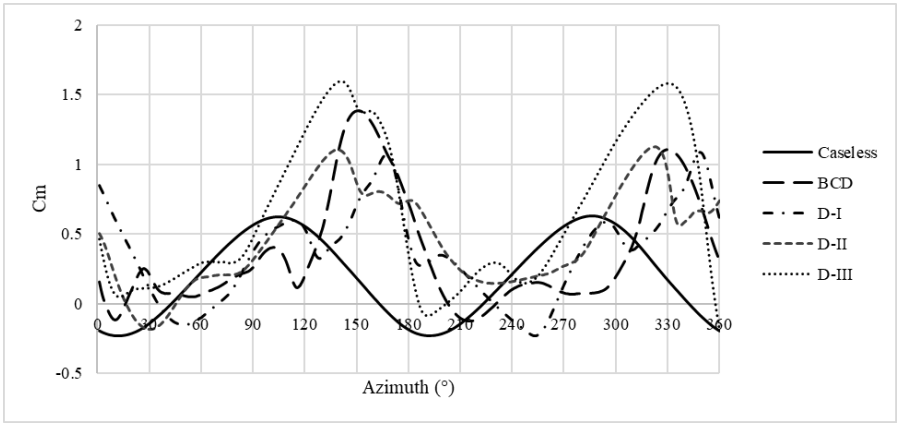

Figure 5. *Cm* vs Azimuth Position of Turbine in a Full Rotation

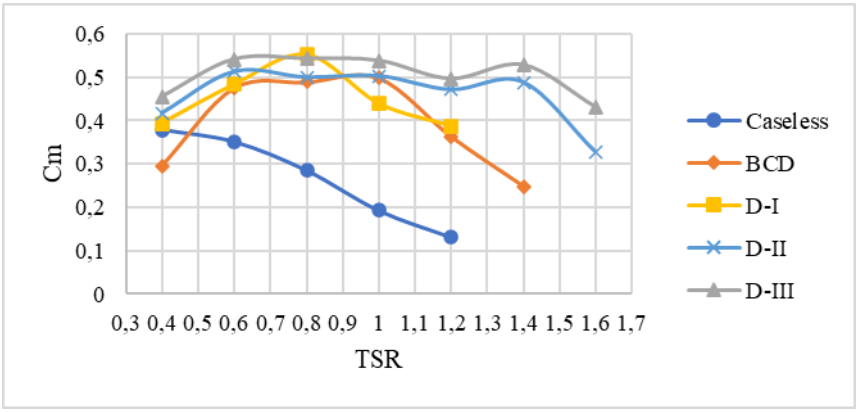

Figure 5. Average *Cm* vs TSR

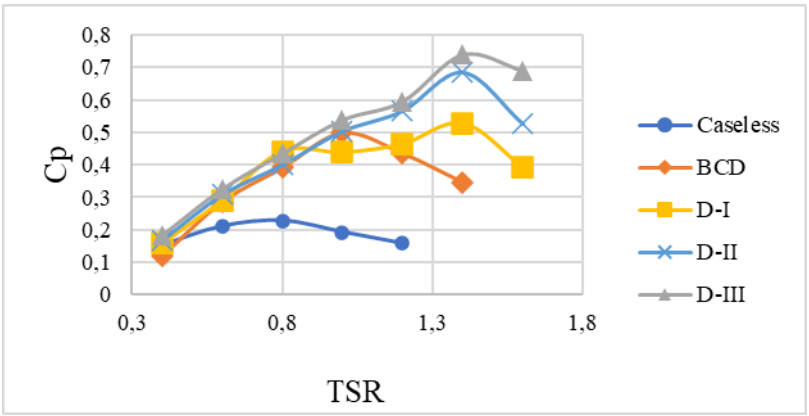

Figure 6. *Cp* vs TSR

C. Coefficient of Power

Figure 6 demonstrates turbine efficiency in terms of power coefficient (*Cp*) of all designs at particular *TSR*'s. It's clear that turbines with casing utilization possess better performance than the caseless design. Caseless design shows maximum *Cp* of 0.23 At *TSR* = 0.8. At low *TSR*, 0.4, BCD has lower *Cp* than caseless turbine. This is in accordance with the previous works by [7]. However, this design possesses a peak *Cp* at *TSR* 1 with 0.50 of *Cp* which is more than twice of caseless turbine's max *Cp*. D-I experiences several intersections with BCD curve. In some *TSR*'s, it provides better performance than BCD. Its peak *Cp* is 0.53 at *TSR* 1.4 which is higher than BCD's max *Cp*. D-II and D-III show similar trends and reach their peaks at *TSR* = 1.4 with *Cp* of 0.73 and 0.68 respectively. D-III's performance stands over other designs at all *TSR*'s except at *TSR* 0.8 where D-I slightly overtook it. Moreover, D-III owns higher *Cp* than BCD's at *TSR*=1 by 8% and higher *Cp* than caseless design at *TSR* = 0.8 by 90%.

D. Fluid Behavior Analysis

In order to get more insights, two points of azimuth position which are 300° and 330° of caseless turbine, BCD, and D-III casing designs are taken as an example to be observed those pressure and velocity fields. Pressure difference between upstream and downstream area of turbine is due to fluid flow behavior where on the front side of the turbine, fluid straight hit the blades

while on another side the flow is separated and creates wake (following blade motion). This pressure difference leads to generate torque. If the difference at the advancing turbine higher than the returning blade, the turbine produces positive torque. But, if higher pressure difference happens on the returning blade than the advancing one, turbine motion could be slowed down as the result of negative torque.

Figure 7 depicts the pressure field of caseless turbine. There is slightly pressure difference on the turbine sides. Thus, the torque produced is relatively low. On the other hand, turbine with installed casing makes higher pressure difference as shown in Figure 8 and Figure 9. This occurrence could happen as a consequence of stagnation effect where the fluid flow strikes turbine blade and its velocity drops dramatically. This behavior can be seen in Figure 10 and Figure 11. The process causes the rise of pressure. In BCD, at 300°, In contrast, *Cm* is lower than the caseless turbine. The discharge stream coming from lower plate result in high pressure on returning blade convex side as presented in Figure 8a. Thus, the turbine rotation is hindered. In casing D-III, this phenomenon does not occur because the stream direction from lower plate passage adds more pressures on advancing blade rather than on returning blade. Hence, it has higher *Cm* as depicted on graph in Figure 9a.

At 330° azimuthal blade position of casing D-III, the blade blocks almost entirely the flow entering the casing, pictured in Figure 11b. This causes the highest pressure difference on turbine sides (see Figure 9b) and hence produces peak *Cm*. The BCD, otherwise, does not block all the flows since the lower plate guides the flow to the concave side of the returning blade, shown in Figure 10b. As the result, pressure difference on advancing blade is much higher than on the returning blade as revealed in Figure 8b. This leads to rise the *Cm* into its peak.

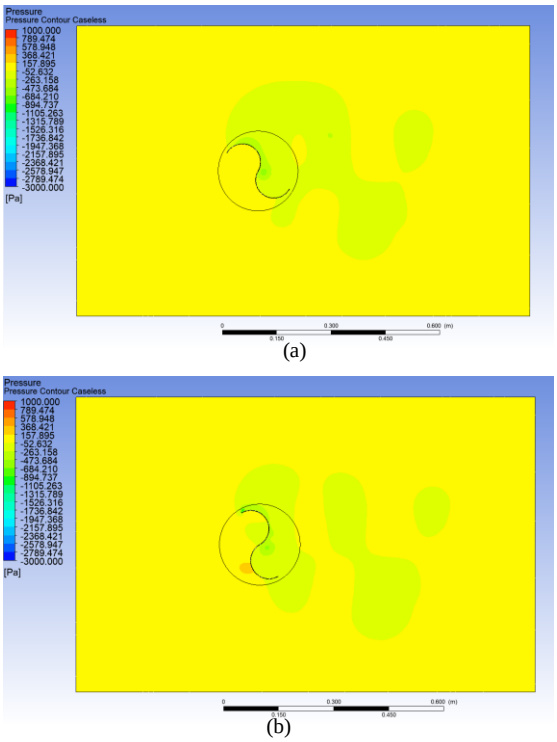

(a)

(b)

Figure 7. Pressure Contour of Caseless Turbine at Azimuth Position of (a) 300° and (b) 330°

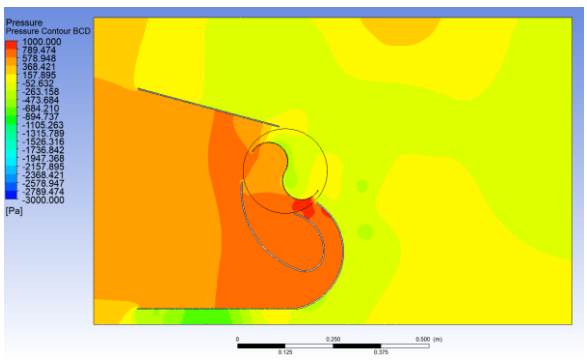

(a)

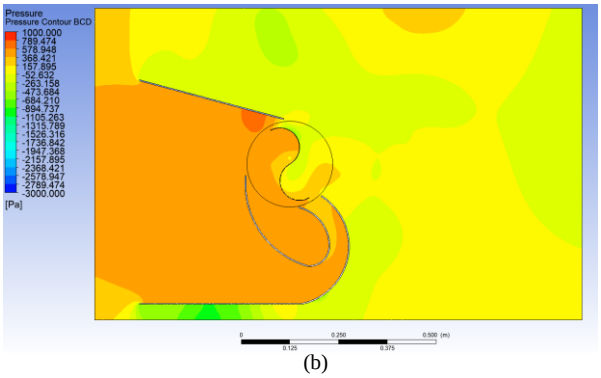

(b)

Figure 8. Pressure Contour of Turbine Utilizing BCD at Azimuth Position of (a) 300° and (b) 330°

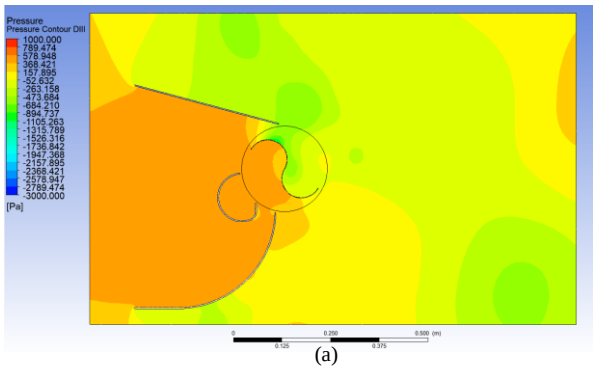

(a)

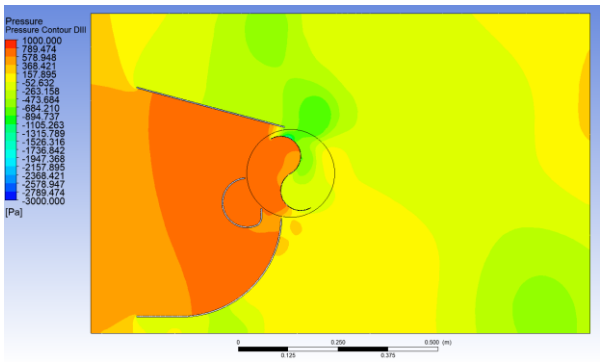

(b)

Figure 9. Pressure Contour of Turbine Utilizing D-III Casing at Azimuth Position of (a) 300° and (b) 330°

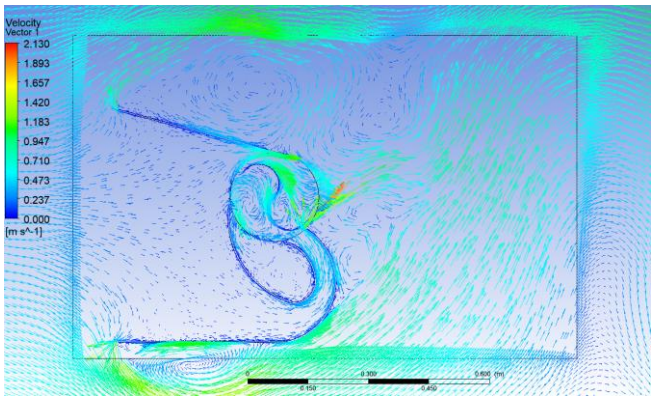

(a)

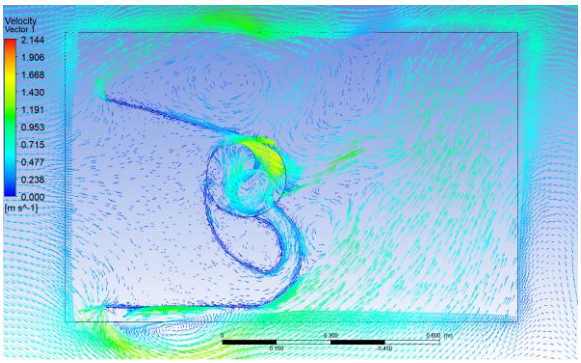

(b)

Figure 10. Velocity Vektor of Turbine Utilizing BCD at Azimuth Position of (a) 300° and (b) 330°

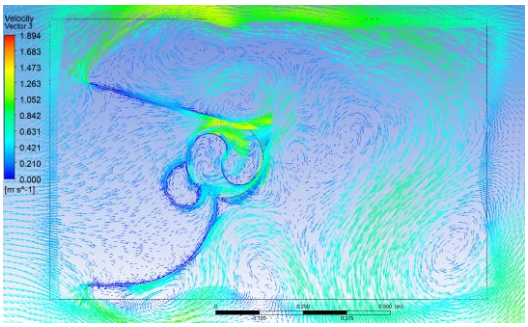

(a)

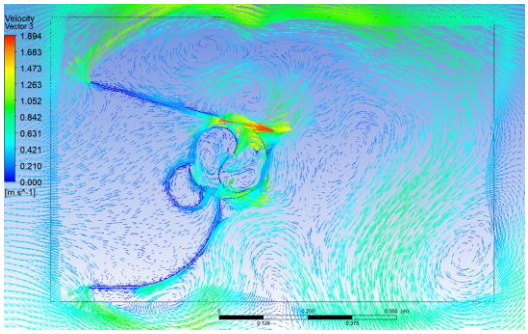

(b)

Figure 11. Velocity Vektor of Turbine Utilizing D-III Casing at Azimuth Position of (a) 300° and (b) 330°

TABLE 1.
VELOCITY AT LOWER PLATE OUTLET

Casing Design	Velocity of Impinging Jet Discharge (m/s)	
	Average	Maximum
BCD	0.540	0.718
I	0.508	0.787
II	0.460	0.786
III	0.458	0.792

Another measurement has been done by placing observation point on outlet of lower plate passage to get velocity data. The results show that shorter passage in all proposed casing designs could increase the maximum velocity of the jet stream (see Table 1). Casing D-III produces the highest velocity jet stream as its passage is the shortest one. The average value, in contrast, depends on the discharge of impinging jet position. The reason of this is because at some turbine azimuth position, the flow coming from upstream and lower passage are blocked by the turbine as discussed above.

IV. CONCLUSION

Three proposed casing designs and a base casing design from previous work were investigated. The results were then compared with each other to evaluate the impact of the modifications. The results reveal that the utilization of casings on a Savonius turbine can improve its performance. The proposed designs D-III and D-II, which have a lower plate guiding the fluid perpendicularly toward the concave side of the returning blade when the blade position is at 90° and 75°, respectively, provide better performance than the

previous casing design across all TSRs. However, the Cp curve of D-I shows several intersections. D-III outperforms the best Cp of the previous casing design by 8% at TSR = 1. By applying the D-III casing design, the best performance of the conventional turbine, with a Cp of 23%, increases to 43% under the same operating condition (TSR = 8). Furthermore, it is found that a shorter flow passage can increase the impinging jet stream velocity

REFERENCES

[1] N. R. Maldar, C. Y. Ng, and E. Oguz, "A review of the optimization studies for Savonius turbine considering hydrokinetic applications," *Energy Conversion and Management*, vol. 226, p. 113495, Dec. 2020, doi: 10.1016/j.enconman.2020.113495.

[2] H. Alizadeh, M. H. Jahangir, and R. Ghasempour, "CFD-based improvement of Savonius type hydrokinetic turbine using optimized barrier at the low-speed flows," *Ocean Engineering*, vol. 202, p. 107178, Apr. 2020, doi: 10.1016/j.oceaneng.2020.107178.

[3] M. Mosbahi, "Performance study of a Helical Savonius hydrokinetic turbine with a new deflector system design," *Energy Conversion and Management*, vol. 194, no. Query date: 2024-10-01 09:59:02, pp. 55–74, 2019, doi: 10.1016/j.enconman.2019.04.080.

[4] P. Setiawan, "Numerical simulation on improvement of a Savonius vertical axis water turbine performance to advancing blade side with a circular cylinder diameter variations," *IOP Conference Series: Earth and Environmental Science*, vol. 200, no. 1, 2018, doi: 10.1088/1755-1315/200/1/012029.

[5] W. A. El-Askary, M. H. Nasef, A. A. AbdEL-hamid, and H. E. Gad, "Harvesting wind energy for improving performance of Savonius rotor," *Journal of Wind Engineering and Industrial Aerodynamics*, vol. 139, pp. 8–15, Apr. 2015, doi: 10.1016/j.jweia.2015.01.003.

[6] N. Thakur, A. Biswas, Y. Kumar, and M. Basumatary, "CFD analysis of performance improvement of the Savonius water turbine by using an impinging jet duct design," *Chinese Journal of Chemical Engineering*, vol. 27, no. 4, pp. 794–801, Apr. 2019, doi: 10.1016/j.cjche.2018.11.014.

[7] E. Antar and M. Elkhoury, "Parametric sizing optimization process of a casing for a Savonius Vertical Axis Wind Turbine," *Renewable Energy*, vol. 136, pp. 127–138, Jun. 2019, doi: 10.1016/j.renene.2018.12.092.

[8] L. A. Gallo, E. L. Chica, E. G. Flórez, and F. A. Obando, "Numerical and Experimental Study of the Blade Profile of a Savonius Type Rotor Implementing a Multi-Blade Geometry," *Applied Sciences*, vol. 11, no. 22, Art. no. 22, Jan. 2021, doi: 10.3390/app112210580.

[9] B. D. Altan and M. Atılgan, "An Experimental And Numerical Study On The Improvement Of The Performance Of Savonius Wind Rotor," *Energy Conversion and Management*, vol. 49, no. 12, pp. 3425–3432, Dec. 2008, doi: 10.1016/j.enconman.2008.08.021.

[10] A. Kumar, "Performance analysis of a Savonius hydrokinetic turbine having twisted blades," *Renewable Energy*, vol. 108, no. Query date: 2024-10-01 09:59:02, pp. 502–522, 2017, doi: 10.1016/j.renene.2017.03.006.

[11] N. Sarma, "Experimental and computational evaluation of Savonius hydrokinetic turbine for low velocity condition with comparison to Savonius wind turbine at the same input power," *Energy Conversion and Management*, vol. 83, no. Query date: 2024-10-01 09:59:02, pp. 88–98, 2014, doi: 10.1016/j.enconman.2014.03.070.

[12] S. Roy and A. Ducoin, "Unsteady analysis on the instantaneous forces and moment arms acting on a novel Savonius-style wind turbine," *Energy Conversion and Management*, vol. 121, pp. 281–296, Aug. 2016, doi: 10.1016/j.enconman.2016.05.044.

[13] W. Tian, B. Song, J. H. VanZwieten, and P. Pyakurel, "Computational Fluid Dynamics Prediction of a Modified Savonius Wind Turbine with Novel Blade Shapes," *Energies*, vol. 8, no. 8, Art. no. 8, Aug. 2015, doi: 10.3390/en8087915.

[14] A. Rezaeiha, I. Kalkman, and B. Blocken, "CFD simulation of a vertical axis wind turbine operating at a moderate tip speed ratio: Guidelines for minimum domain size and azimuthal increment," *Renewable Energy*, vol. 107, pp. 373–385, Jul. 2017, doi: 10.1016/j.renene.2017.02.006.

[15] N. Alom, U. K. Saha, and A. Dewan, "In the quest of an appropriate turbulence model for analyzing the aerodynamics of a conventional Savonius (S-type) wind rotor," *Journal of Renewable and Sustainable Energy*, vol. 13, no. 2, p. 023313, Apr. 2021, doi: 10.1063/5.0034362.

[16] A. Dewan, S. S. Tomar, A. K. Bishnoi, and T. P. Singh, "Computational fluid dynamics and turbulence modelling in various blades of Savonius turbines for wind and hydro energy: Progress and perspectives," *Ocean Engineering*, vol. 283, p. 115168, Sep. 2023, doi: 10.1016/j.oceaneng.2023.115168.

[17] S. Roy and U. K. Saha, "Computational Study to Assess the Influence of Overlap Ratio on Static Torque Characteristics of a Vertical Axis Wind Turbine," *Procedia Engineering*, vol. 51, pp. 694–702, Jan. 2013, doi: 10.1016/j.proeng.2013.01.099.

[18] S. V. Ghatage and J. B. Joshi, "Optimisation of vertical axis wind turbine: CFD simulations and experimental measurements," *The Canadian Journal of Chemical Engineering*, vol. 90, no. 5, pp. 1186–1201, 2012, doi: 10.1002/cjce.20617.

[19] A. Goude and O. Ågren, "Simulations of a vertical axis turbine in a channel," *Renewable Energy*, vol. 63, pp. 477–485, Mar. 2014, doi: 10.1016/j.renene.2013.09.038.

[20] P. K. Talukdar, A. Sardar, V. Kulkarni, and U. K. Saha, "Parametric analysis of model Savonius hydrokinetic turbines through experimental and computational investigations," *Energy Conversion and Management*, vol. 158, pp. 36–49, Feb. 2018, doi: 10.1016/j.enconman.2017.12.011.

[21] M. H. Nasef, W. A. El-Askary, A. A. AbdEL-hamid, and H. E. Gad, "Evaluation of Savonius rotor performance: Static and dynamic studies," *Journal of Wind Engineering and Industrial Aerodynamics*, vol. 123, pp. 1–11, Dec. 2013, doi: 10.1016/j.jweia.2013.09.009.

[22] M. Badrul Salleh, N. M. Kamaruddin, P. How Tion, and Z. Mohamed-Kassim, "Comparison of the power performance of a conventional Savonius turbine with various deflector configurations in wind and water," *Energy Conversion and Management*, vol. 247, p. 114726, Nov. 2021, doi: 10.1016/j.enconman.2021.114726.